Third International Conference on CFD in the Minerals and Process Industries
CSIRO, Melbourne, Australia
10-12 December 2003

SIMULATION OF TURBULENT FLOW IN A CYCLONIC SEPARATOR

Stefan SCHMIDT, Hugh M. BLACKBURN, Murray RUDMAN and Ilija SUTALO

CSIRO Manufacturing and Infrastructure Technology
PO Box 56, Highett, Victoria, 3190 AUSTRALIA

ABSTRACT

In this paper the turbulent flow in a cyclonic separator is investigated with large-eddy simulation (LES) based on a cylindrical coordinate spectral-element-Fourier method (SEM) using the Smagorinsky subgrid-scale model in its standard and dynamic formulation. The results show slight model differences, but both have poor agreement with measurements. The cylindrical-coordinate system geometry used in the SEM-Fourier calculations requires periodicity in the azimuthal direction and cannot model the inflow duct. Hence the flow velocity profiles have to be interpolated onto the intersection of inflow duct and main cyclone wall. A comparison based on a full three-dimensional finite-volume method (FVM) indicates that the inclusion of some portion of the inflow duct in the geometry improves the agreement to experimental results.

NOMENCLATURE

∇	gradient operator $[1/m]$
$\overline{\phi}, \widehat{\phi}$	resolved quantity ϕ on grid filter level and test filter level
C_S	Smagorinsky constant [1]
Δ	local grid spacing $[m]$
$\boldsymbol{I}$	identity tensor [1]
l, v	length scale $[m]$, velocity scale $[m/s]$
l_S	mixing-length $[m]$
$\boldsymbol{\mathcal{L}}$	auxiliary tensor $[m^2/s^2]$
$\boldsymbol{\mathcal{M}}$	auxiliary tensor $[1/s^2]$
ν_t	eddy viscosity $[m^2/s]$
$\boldsymbol{S}, S_{ij}$	strain rate tensor and its components $[1/s]$
$\boldsymbol{\tau}, \boldsymbol{T}$	turbulent shear stress on grid and test filter level $[N/m^2]$
$\boldsymbol{u}$	velocity vector $[m/s]$
u_i, u_i'	instantaneous velocity and fluctuating velocity component $[m/s]$
α	half-angle of cyclone [1]
N	number of grid points [1]
R, D	outer radius/diameter of cyclone $[m]$
Re	Reynolds number [1]
$r_\mathrm{vf}, d_\mathrm{vf}$	radius/diameter of vortex finder $[m]$
r_c	radius of axisymmetric centre body $[m]$
Tu	turbulence level [1]
U_0	inflow velocity $[m/s]$
U, V, W	time-averaged velocities $[m/s]$
x, y, z	Cartesian coordinates $[m]$
z_0	location of intersection of parallel and conical part of cyclone $[m]$
z^*	normalised axial coordinate $[m]$

INTRODUCTION

Cyclones play a dominant role in the industrial separation of dilute particles from an incoming gas flow. The incoming flow enters the constant-diameter part of the cyclone tangentially and accelerates on its way down into the conical section resulting in a strong swirling flow with complex flow patterns. At the base, the particle-laden under-flow escapes through the lower end, while the rest reverses direction and swirls along the centreline through the vortex-finder pipe of the cyclone towards the top out-flow.

In this study the bottom escape is closed as the main objective of this study is to investigate the single-phase 'carrier' flow, which is supposed to leave through the top of the domain. The actual size and the half-angle α of the cyclone are determined by the given particle size d to be separated from the incoming mixture (Griffiths and Boysan, 1996; Hoffmann and Stein, 2002). Consequently the amount of swirl and the pressure loss in the cyclone may vary depending on the actual design and shape.

Turbulence Models

The large swirl velocity produces difficulties for simple statistical turbulence models employed in typical Reynolds-Averaged Navier–Stokes equation (RANS) approaches such as the $k-\varepsilon$ model which is still widely used in industrial design. The simple linear stress-strain correlations in these models often fail in the presence of streamline curvature accompanied by swirl. This failure of the models often gives rise to swirl velocity profiles typical of solid-body rotation. This sort of modelling error can be alleviated by including non-linear correlations of rate-of-strain S_{ij} and rate-of-rotation Ω_{ij} tensors (Rung, 2000). Moreover, sophisticated models such as some ASM with special treatment of coriolis forces (Rung, 2000) and full implicit Reynolds stress transport models achieve a better performance for swirling flows. However, as this paper aims at investigating the model influence in LES we do not consider second-moment closures here.

Smaller modelling errors are to be expected from LES, which directly resolves the large-scale flow structures, which carry most of the kinetic energy and which models the influence of small scales, below the grid level using a simple subgrid-scale model. The distinction between super- and subgrid scales is achieved by a convolution of the Navier–Stokes equations with a filter kernel, resulting in a set of filtered Navier–Stokes equations which include a residual stress tensor known as true subgrid-scale stresses, that has to be modelled using philosophies

similar to those employed in producing RANS models.

In wall bounded flows much of the important physics occurs in the boundary layer and this region needs to be adequately dealt with, either through high resolution (for wall-resolving LES and direct numerical simulation, DNS) or by a model. Wall-resolving LES demands spatial resolution in the wall layers approaching that required for DNS and becomes infeasible for very high-Reynolds number flows. RANS on the other hand employs wall models to bypass the wall layer, but is not able to distinguish between time-scales of transient motion and turbulence. This gave rise to the development of hybrid approaches such as detached-eddy simulation (DES, Spalart et al., 1997), which uses standard RANS wall modelling in conjunction with LES for all detached eddies using a modification of the Spalart-Allmaras (SA) RANS model (Spalart and Allmaras, 1994) which basically limits the length scale based on the local grid spacing. Thus, it is able to resolve transient flow features without the need to fully resolve the wall region. This method allows a substantial reduction of the computational effort and gives similar results as marginally resolved LES (Schmidt and Thiele, 2002a/2002b).

Subgrid-Scale Model

For the spectral element method, both the standard and dynamic Smagorinsky model have been implemented and validated for the channel flow (Blackburn and Schmidt, 2002). The standard Smagorinsky model (SM) determines the unknown stresses $\boldsymbol{\tau} = -2\,\nu_\mathrm{t}\,\overline{\boldsymbol{S}}$ by a length scale $l = \overline{\Delta}$ and a velocity scale $v = \overline{\Delta}\,|\overline{\boldsymbol{S}}|$ with $|\overline{\boldsymbol{S}}| = (2\,\overline{\boldsymbol{S}}{:}\overline{\boldsymbol{S}})^{1/2}$, $\overline{\boldsymbol{S}} = [\nabla\overline{\boldsymbol{u}} + (\nabla\overline{\boldsymbol{u}})^T]/2$ and a constant to give

$$\nu_\mathrm{t} \approx l\,v \quad = (C_\mathrm{S}\overline{\Delta})^2\,|\overline{\boldsymbol{S}}|\,. \tag{1}$$

The dynamic model (DSM, (Germano et al., 1991; Lilly, 1992) makes use of the general relation ('Germano's identity')

$$\boldsymbol{\mathcal{L}} = \boldsymbol{T} - \widehat{\boldsymbol{\tau}} \tag{2}$$

to link the stresses at grid-level $\boldsymbol{\tau}$ and test level $\boldsymbol{T}$, obtained by the application of two different filter kernels $\overline{\Delta}$ and $\widehat{\overline{\Delta}}$ to the unfiltered Navier–Stokes equations. The assumption of scale-similarity at both cut-off wave numbers allows using the same subgrid-scale model with the same model coefficient

$$\begin{aligned} \boldsymbol{\tau} - \frac{1}{3}\,\mathrm{tr}(\boldsymbol{\tau})\,\boldsymbol{I} &= -2\,(C_\mathrm{S}\,\overline{\Delta})^2\,|\overline{\boldsymbol{S}}|\,\overline{\boldsymbol{S}} \\ \boldsymbol{T} - \frac{1}{3}\,\mathrm{tr}(\boldsymbol{T})\,\boldsymbol{I} &= -2\,(C_\mathrm{S}\,\widehat{\overline{\Delta}})^2\,|\widehat{\overline{\boldsymbol{S}}}|\,\widehat{\overline{\boldsymbol{S}}}\,. \end{aligned}$$

Introducing these equations into the deviatoric components of (2) gives

$$\boldsymbol{\mathcal{L}} - \frac{1}{3}\,\mathrm{tr}(\boldsymbol{\mathcal{L}})\,\boldsymbol{I} = -2\,(C_\mathrm{S}\,\overline{\Delta})^2\boldsymbol{\mathcal{M}} \tag{3}$$

with

$$\boldsymbol{\mathcal{M}} = \left(\frac{\widehat{\overline{\Delta}}}{\overline{\Delta}}\right)^2 |\widehat{\overline{\boldsymbol{S}}}|\,\widehat{\overline{\boldsymbol{S}}} - \widehat{|\overline{\boldsymbol{S}}|\,\overline{\boldsymbol{S}}}\,, \tag{4}$$

where typically $\widehat{\overline{\Delta}}/\overline{\Delta} = 2$ is assumed. In order to obtain a scalar dynamic estimate, the tensor equation (3) is reduced by double contraction (Lilly, 1992), which process the isotropic component of $\boldsymbol{\mathcal{L}}$ is eliminated, since $\boldsymbol{\mathcal{M}}$ is deviatoric

$$\boldsymbol{\mathcal{L}}{:}\boldsymbol{\mathcal{M}} = -2\,(C_\mathrm{S}\,\overline{\Delta})^2\boldsymbol{\mathcal{M}}{:}\boldsymbol{\mathcal{M}}\,, \tag{5}$$

from which the dynamic estimate can be extracted

$$l_\mathrm{S}^2 = \left(C_\mathrm{S}(\boldsymbol{x},t)\,\overline{\Delta}\right)^2 = -\frac{1}{2}\,\frac{\boldsymbol{\mathcal{L}}{:}\boldsymbol{\mathcal{M}}}{\boldsymbol{\mathcal{M}}{:}\boldsymbol{\mathcal{M}}}\,. \tag{6}$$

This procedure evaluates a local and time-dependent value of $(C_\mathrm{S}\,\overline{\Delta})$ and is updated every time step. Note that the product $(C_\mathrm{S}\,\overline{\Delta})$ can be treated as a mixing length l_S, without explicitly specifying the length scale on the grid level—this is advantageous in complex geometries as it enables us to bypass the need to define $\overline{\Delta}$. The dynamic estimate (6) can generate locally negative values of the eddy viscosity ν_t, which, if persistent, can destabilise the time-integration procedure. In the present computations the mixing length is limited to $|(l_\mathrm{S}/\overline{\Delta})^2| < C_\mathrm{S}^2$.

NUMERICAL METHOD

The LES are carried out with a spectral element method. For comparison additional DES and RANS computations based on the SA model were performed with a three-dimensional finite-volume method to cross-check the LES results.

Spectral Element Method

The spatial discretisation employs a spectral element–Fourier formulation (Blackburn and Schmidt, 2002), which allows arbitrary geometry in the (z,r) plane to be represented using a spectral-element discretisation, but requires periodicity in the θ direction. The basis of the method as applied to the direct numerical simulation of the incompressible Navier–Stokes equations in a cylindrical coordinate system has been described by Blackburn and Lopez (2002).

As a result of the Fourier decomposition, implementation of the time integration as a parallel algorithm is straightforward, with inter-process communication required only during formulation of the nonlinear terms. The message-passing kernel MPI has been used for this operation, and the computations reported here were carried out using 8-16 processors.

Finite-Volume Method

The Navier–Stokes equations are discretized using a cell-centered pressure-based finite-volume method employing on semi-structured grids (Xue, 1998). Diffusive fluxes are approximated by a 2nd order central-differencing scheme (CDS). In LES, also convective fluxes are approximated by the CDS whereas for RANS and DES these fluxes are discretized using upwind-biased bounded high-order schemes. The fully implicit three-level time integration (2nd order accuracy) ensures CFL stability even in coarse regions of the mesh, where the CDS would produce unphysical solutions due to high Peclet numbers. The flow solver is parallelised using a blockwise domain decomposition technique employing message passing libraries MPI for inter-block communication.

FLOW CONFIGURATION

The cyclone (Fig. 1a) features an outer diameter $D = 2\,R$ and a half-angle of $\alpha = 20^o$ in the conical region and a pipe at the bottom end for collecting particles. As mentioned earlier, this outflow is closed for all simulations. Hence only the main outflow through the vortex finder with diameter d at the top of the cyclone is used. The Reynolds number based on the bulk inflow velocity U_0 and the diameter D of the cyclone is $Re = 10^6$.

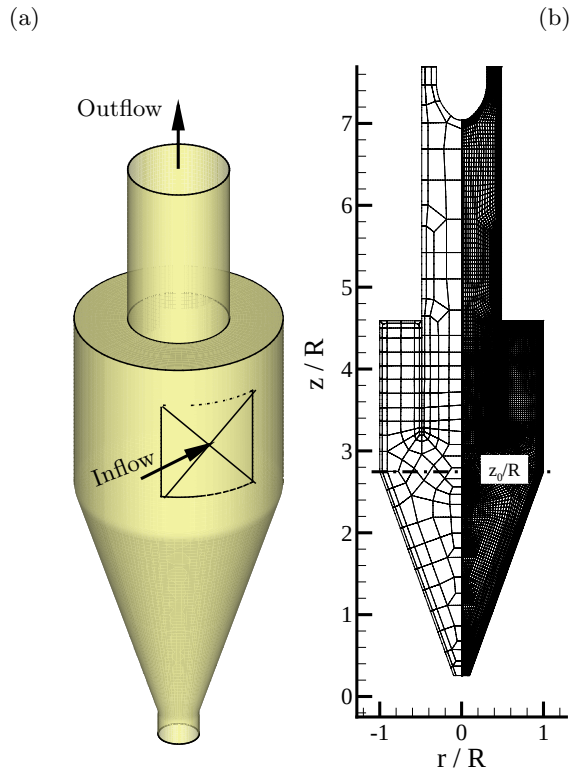

Figure 1: Cyclone geometry (a) without inflow duct and (b) element boundaries with 2D projection of the underlying mesh as used by spectral-element method calculations.

Boundary Conditions

As the cylindrical spectral-element-Fourier method requires the azimuthal direction to be periodic in geometry, the inflow duct of the cyclone cannot be represented. For this reason, velocity profiles obtained from a full three-dimensional simulation (FVM) which included the inflow duct have been interpolated onto the intersection plane of duct and parallel part of the main cyclone. Using constant inlet velocity profiles turned out to be a too coarse approximation of the reality and therefore these are not employed here. However, even with the more representative inlet velocity profiles, steady velocities enter this intersection surface, leading to an inflow turbulence level of Tu=u'/U_0=0%. This partly suppresses the natural interaction of the incoming flow and the unsteady turbulent flow in the cyclone. The introduction of random noise ($u' \approx 0.1\ U_0$) does not significantly improve the results, as these pseudo-turbulent velocities do not represent realistic flow patterns in the inflow duct.

The vortex finder ($d_{\mathrm{vf}} = 2r_{\mathrm{vf}}$) was extended to $z/R > 7.5$ in the present computations and an axis-symmetric centre body ($r_c/r_{\mathrm{vf}} \leq 0.63$) was placed into the outflow plane to avoid inflow occurring at the outflow close to the centreline (Fig. 1b). Hence the flow was allowed to leave the domain between $0.63 < r/r_{\mathrm{vf}} < 1.0$ ($0.3 < r/R < 0.5$). This outflow insert is unlikely to substantively influence the flow more than a few vortex finder diameters upstream.

Computational Mesh

The mesh structure in the (z, r) plane is shown on the left half of figure (1b); on the right half the nodal points of the underlying mesh are displayed, showing the refinement of the mesh in all near wall regions, particularly of the vortex finder tube in the centre of the cyclone. The LES mesh comprises of 230 spectral elements of 8×8 tensor-product shape functions and 96 azimuthal planes in the Fourier direction leading to roughly $N \approx 1.4 \times 10^6$ nodes. The near wall-normal grid spacing reach values above $y^+ > 10$ in critical parts of the geometry. As wall-functions were not used in the computations, the present results can hardly be regarded as wall-resolving LES. However, as the main flow features are governed by the internal vortical structure and not primarily determined by the near-wall turbulence, it is hoped that this lack of resolution does not unduly influence the results. In spite of this shortcoming, we should be able to draw at least some basic conclusions about the influence of the subgrid-scale model.

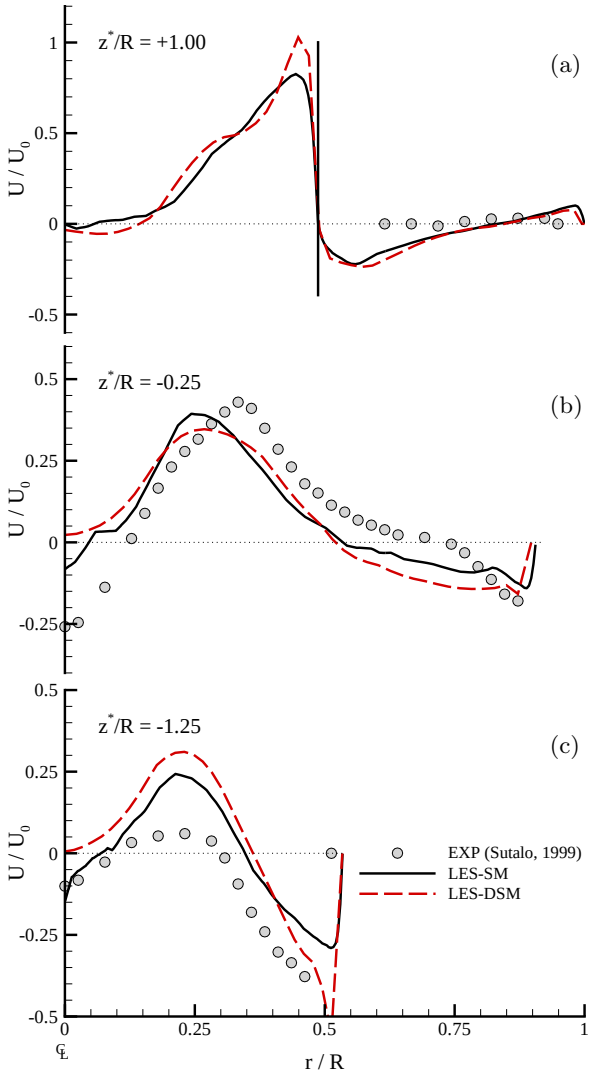

Figure 2: Time-averaged axial velocity profiles at: (a) $z^*/R = 1.0$, (b) $z^*/R = -0.25$ and (c) $z^*/R = -1.25$; the vertical line in picture (a) indicates the position of the vortex finder.

EXPERIMENTS

In laser-Doppler anemometry (LDA, Sutalo and Mer-

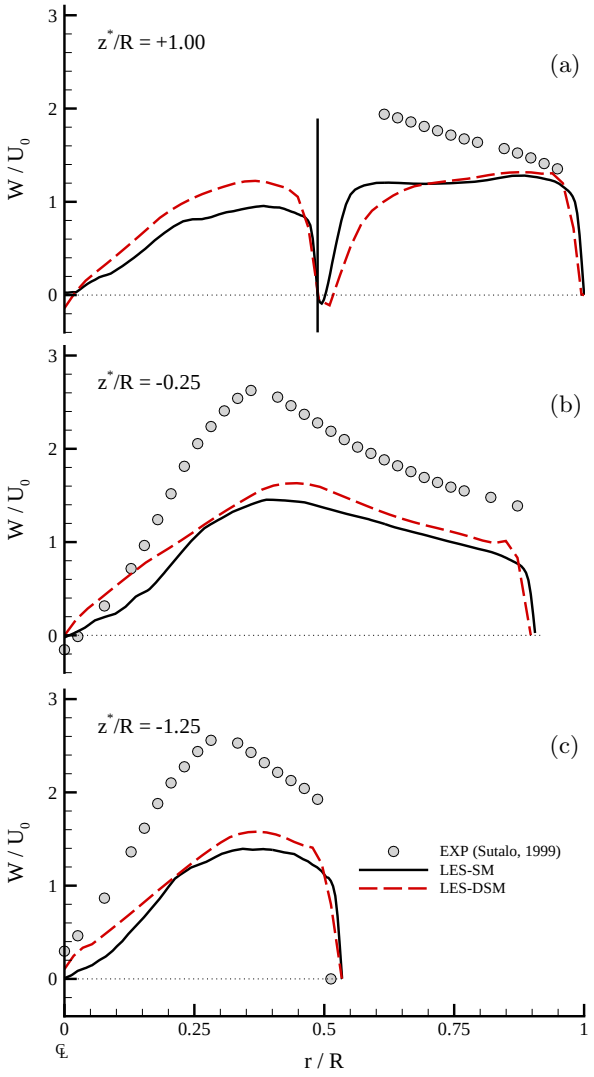

Figure 3: Time-averaged tangential velocity profiles at: (a) $z^*/R=1.0$, (b) $z^*/R=-0.25$ and (c) $z^*/R=-1.25$; the vertical line in picture (a) indicates the position of the vortex finder.

rell, 1999) both averaged mean and fluctuating velocities in the tangential and the axial direction have been taken on the semi-plane ($r/R > 0$) located $\varphi = 90^o$ downstream of the semi inlet-plane. Velocity data could not be obtained inside the vortex finder. As no time series was recorded during the experiment, no correlations or energy spectra can be extracted.

RESULTS

Figures 2 and 3 show the time-averaged mean axial and tangential velocity profiles at three different locations $z^* = z - z_0$ counted from the joint of the parallel and conical part of the cyclone $z_0/R = 2.745$ (cf. Fig. 1b), from the experiments and from the spectral element based LES. Taken overall, the results using steady inflow conditions indicate that while the time-averaged axial velocities are modelled with reasonable success, the time-averaged swirl velocities, while having the correct profile shape, are substantially too low compared to the experimental results (Sutalo and Merrell, 1999). While the dynamic LES provides slightly better matching of the swirl velocities, the influence of subgrid scale treatment is not substantial.

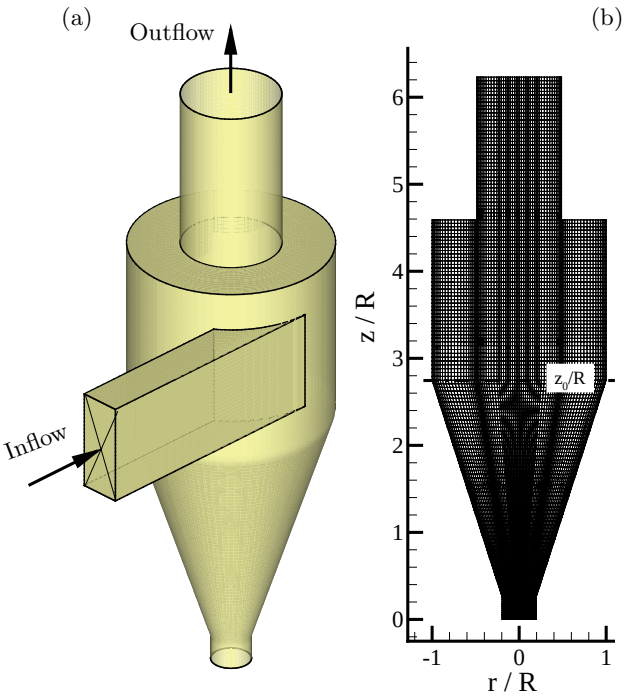

Figure 4: Cyclone geometry and block-structured grid as used by finite-volume method calculations.

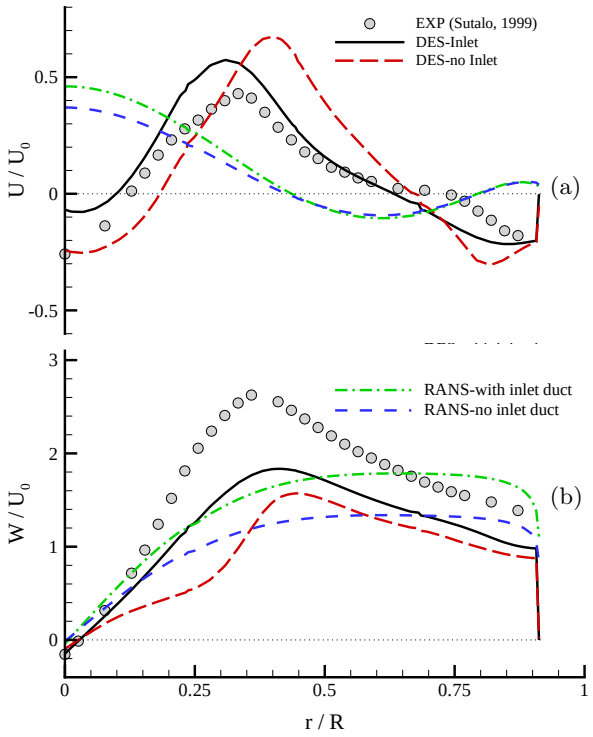

Figure 5: Influence of inflow boundary condition: Time-averaged velocity profiles at $z^*/R=-0.25$: (a) axial velocity and (b) tangential velocity.

Influence of Inflow Boundary Conditions

One key factor causing the lack of agreement of the swirl velocity was thought to be the crude approximation of the inflow boundary conditions at the inflow to the cyclone. For comparison, a full three-dimensional mesh including the inflow duct consisting of $N \approx 500\,000$ control volumes was generated (Fig. 4) and simulated by DES and RANS using the previously described FVM.

In Figure 5 the results of DES and RANS using the SA model obtained on both geometries (Figs. 1a/4a) are shown. As expected, the DES results are broadly similar to the LES results, but differ in important details. The DES based on the geometry including the inflow duct (Fig. 4a) reveal that the inflow boundary condition indeed has a strong influence on the results. At $z^*/R = -0.25$, the axial velocities (Fig. 5a) are quite different; results on the full geometry give a better agreement with the experiments than the DES results obtained on the same geometry as the LES. However, the swirl velocity (Fig. 5b) only marginally improves and is still too low by more than 30%.

The results obtained by RANS reveal two facts. First is that this simple model fails to capture the correct swirl velocity distribution and predicts totally incorrect axial velocity distributions which seem not to be influenced by the type of inflow. The second fact is that despite this discrepancy the swirl component is influenced by the inflow conditions to a similar extent as the DES results.

DISCUSSION AND CONCLUSIONS

A cross check of two experimental data sets confirmed that the current measurements are repeatable to within 10%. Therefore, other reasons must be responsible for the lack of agreement with the experiments.

The LES results of the cyclone reveal reasonable success in predicting the axial velocity but on the other hand achieve comparatively poor agreement of the swirl velocity. As the influence of the subgrid-scale model in the LES results is quite small, turbulence modelling errors are not likely to have caused this discrepancy. While the near-wall resolution is often to low, for wall-resolving LES (in the spectral-element simulations), it should be adequate in the case of the DES and RANS calculations. The most likely reason for the discrepancy between the experimental and LES/DES swirl velocities is thought to be related to insufficient spatial resolution in the interior of the cyclone just below the vortex finder (cf. Fig. 1b). In this region the mainly tangential flow is about to enter the conical part of the cyclone, where the swirl velocity reaches its maximum values.

Since the numerical scheme used for LES requires periodicity in the azimuthal direction, the inflow duct was not geometrically modelled in present computations and hence interpolated velocities had to be used as inflow conditions. A comparison based on DES and RANS using a three-dimensional FVM disclosed that indeed the inflow conditions into the cyclone have a strong impact on the development of the swirl velocity. DES employs a modified SA turbulence model and can in fact obtain superior results compared to under-resolved LES. Simple RANS models however fail to predict the correct flow features in the cyclone shown by the standard SA results.

Further work is required and the first step will be the simulation of the full geometry with the three-dimensional finite-volume method with adequate near wall resolution.

ACKNOWLEDGEMENTS

The support of the Australian Partnership for Advanced Computing (APAC) is gratefully acknowledged.

REFERENCES

BLACKBURN, H. and SCHMIDT, S., (2003), Spectral element filtering techniques for large eddy simulation with dynamic estimation, *J. Comput. Phys.*, **186**, 610–629.

BLACKBURN, H. M. and LOPEZ, J. M., (2002), Modulated rotating waves in an enclosed swirling flow, *J. Fluid Mech.*, **465**, 33–58.

GERMANO, M., PIOMELLI, U., MOIN, P. and CABOT, W. H., (1991), A dynamic subgrid-scale eddy viscosity model, *Phys. Fluids*, **A3**, 1760–1765.

GRIFFITHS, W. and BOYSAN, F., (1996), Computational fluid dynamics (cfd) and empirical modelling of the performance of a number of cyclone samplers, *J. Aero. Sci.*, **27**, 281–304.

HOFFMANN, A. and STEIN, L., (2002), *Gas Cyclones and Swirl Tubes*, Springer.

LILLY, D., (1992), A proposed modification of the Germano subgrid-scale closure method, *Phys. Fluids*, **A4**, 633–635.

RUNG, T., (2000), *Entwicklung anisotroper Wirbelzähigkeitsbeziehungen mit Hilfe von Projektionstechniken*, PhD Thesis, Technical University of Berlin.

SCHMIDT, S. and THIELE, F., (2002a), Comparison of numerical methods applied to the flow over wall-mounted cubes, *Intnl J. Heat Fluid Flow*, **23**, 330–339.

SCHMIDT, S. and THIELE, F., (2002b), Detached and large eddy simulation of airfoil flow on semi-structured grids, in *Advances in LES of Complex Flows, Proceedings of the EUROMECH Colloquium 412, Munich, 4.-6.10.2000*, editors R. Friedrich and W. Rodi, Kluwer Academic Publishers, volume 65 of *Fluid Mechanics and its Applications*, 255–272, ISBN 1-4020-0486-9.

SPALART, P. and ALLMARAS, S., (1994), A one-equation turbulence model for aerodynamic flows, *La Rech. Aérospatiale*, **1**, 5–21.

SPALART, P., JOU, W.-H., STRELETS, M. and ALLMARAS, S., (1997), Comments on the feasibility of les for wings, and on a hybrid rans/les approach, in *Advances in DNS/LES*, editors C. Liu and Z. Liu, Greyden Press, Columbus, OH, USA.

SUTALO, I. and MERRELL, J., (1999), Pressure loss measurements on physical models of cyclones, Report 99/095, CSIRO BCE.

XUE, L., (1998), *Entwicklung eines effizienten parallelen Lösungsalgorithmus zur dreidimensionalen Simulation komplexer turbulenter Strömungen* , PhD Thesis, Technical University of Berlin.